

The Performance of Single and Bilayer Graphene: The Initial Study

¹Marriaty Morsin and ²Yusmeeraz Yusof

¹Department of Electrical Engineering, Politeknik Mersing, Jalan Nitar,
86800 Mersing, Johor, Malaysia.

²Department of Electronic and Computer Engineering, Faculty of Electrical Engineering,
Universiti Teknologi Malaysia, 81310 UTM, Johor Bahru, Johor, Malaysia.

*Corresponding Author: marriaty@tvvet.pmj.edu.my

Article Info

Article history:

Article received on 26 June 2023

Received in revised form 06 July 2023

Keywords:

Graphene, single-layer, bilayer,
electronic properties, transconductance

ABSTRACT: Graphene is a viable material for the building of next-generation electronic devices because of its configurable band gap. Graphene's electrical and transport properties are examined in this research for both single- and bilayer forms using Extended-Huckel and Non-Equilibrium Green's Functional (NEGF) simulations. Results from the simulations showed that the band gap opening depends on the arrangement and the layers of the graphene up to 1.701 eV and 1.854 eV for AA-stacked and AB-stacked bilayer graphene respectively. The bilayer graphene transmission spectrum is doubled that of a single layer graphene. AA bilayer has a substantially better conductance and thermal conductivity than other kinds of graphene sheets. The I – V curve shows p-type semiconductor behavior. Likewise, the bilayer graphene shows excellent performance compared to the single-layer device with the AA device showing superior performance than AB by 2.45%.

1. INTRODUCTION

Investigation of the physical and electronic properties of graphene has been tremendously done since its disclosure in 2004 [1]. Several studies had shown the superiority of graphene such as higher electron mobility [1], [2], wide electrical window [2], the bareness of the graphene and exposure directly to liquid [2], high thermal conductance [3], tunable bandgap [2] and zero bandgap [4]. Graphene is extremely competitive in electronics applications due to the Dirac point's conical shape. Pristine graphene devices can have mobility of up to $105 \text{ cm}^2/\text{V}\cdot\text{s}$ [1] as opposed to the mobility of a normal silicon device, which is $\leq 1400 \text{ cm}^2 \text{ V}^{-1}\text{s}^{-1}$. Indeed, graphene has garnered significant attention in the field of sensing and detection through its unique properties [1]. As a 2D material, graphene exhibits exceptional electrical, mechanical, and optical properties that make it highly suitable for sensing applications. The limelight of monolayer graphene has

recently been extended into bilayer and multilayer graphene [5]–[8].

Bilayer graphene has a completely different band structure when one more layer is added to the single layer. Generally, there are two types of graphene stacking. First, the AB-stacked (Bernal-stacked) [6] bilayer graphene system has received a lot of interest due to the fact that it is a stable material and is utilized in popular graphene-based electronics. On the other hand, the AA stacking bilayer graphene (BLG) despite having unique structural characteristics that give it distinct physical properties, is rarely documented. The bandgap for monolayer and bilayer AA-stacked graphene has zero bandgap in the pristine form, however if the symmetry of the two layers is violated in the AB-stacked BLG, a non-zero bandgap may be created. Through an electric field normal to the surface, the bandgap of the BLG is very controllable.

While graphene's physical and electrical properties have been extensively studied, research interest has also

expanded to the conductance, thermal conductance, metal-graphene interfaces such as GFET, and the use of Raman spectroscopy. These areas of investigation contribute towards a greater comprehension of graphene's behavior and enable the development of devices and applications based on graphene [3], [10]–[12]. The study of graphene also included the layers of graphene [7], [13], defects [14]–[17], and many more. The purpose of this study is to acquire better knowledge of how the layers of graphene affect the structure and density of the states, besides analyzing how they affect the transport of carriers through the graphene channels.

In the current work, we provide the extended study of the single-layer graphene and bilayer graphene sheets on the electronic properties of the graphene sheet in the form of graphene device. The performance on bulk single layer defect graphene has being reported previously [18]. The graphene's performance was analyzed in the form of a graphene device. The conductance of single-layer and bilayer graphene, as well as its thermal conductance and transmission spectrum, are given in this study. These readings were made at the 0 Fermi level, 300 K (room temperature). It is believed that the findings from this study will mark yet a distinct pivotal stage in the evolution of graphene.

2. COMPUTATIONAL METHOD AND CALCULATION

2.1. Software and Calculation

The Quantum Wise software was employed in this investigation because it supports device and bulk simulation structures (bulk-nanodevice) [19]. For this simulation purpose, self-consistent Extended-Huckel and Non-Equilibrium Green's Functional (NEGF) methods [20] were employed to investigate the graphene field effect's thermal, electrical, and physical conductivity in device form. In this case, the Huckel basic set elements for graphene were set to carbon with the basic type Cerda carbon (graphite) and a vacuum level of -7.36577 eV. The Recursion calculator was used to calculate the physical parameters of the graphene field effect, such as band structures and transmission spectra, with k-point sampling set to 100. The point per segment of Γ to X, Y, and Z points was set to 200 at the Brillouin zone. The IV curves, conductance, and thermal conductance were all analysed using similar techniques. Multigrid techniques were employed in electrode calculations to resolve the Poisson equation. The k-point sampling was set to 1, 10, and 100 for single-layer graphene, while the bilayer was

set to 2, 10, and 100. The Fermi level (about 0 eV) at temperature settings of 300 K was used to analyse all observed results.

2.2. Model

There are two (2) models involved in the study; 1) the bulk graphene sheet and 2) the graphene device. Figure 1 shows the identical arrangement of three (3) types of bulk graphene sheets that are the single-layer pristine (SLP), the pristine AA-stacked bilayer graphene (AA), and the pristine AB-stacked bilayer graphene (AB). The dimensions settings for the single and double-layer bulk graphene sheets were set to the length of 13.55 \AA and width of 7.91 \AA . In this simulation, the AA and AB spacing was 3.405 \AA which is equal to the spacing in graphite [9].

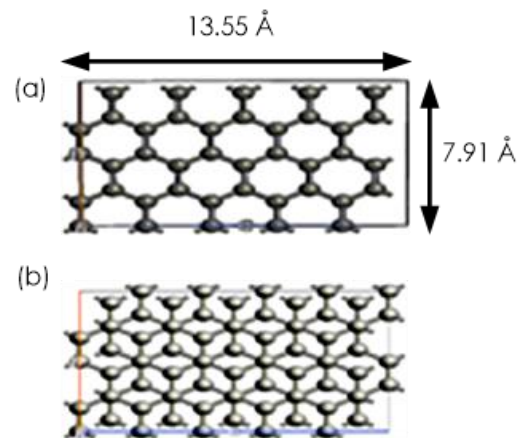


Figure 1: (a) The SLP and AA and (b) AB graphene sheet. Each of the graphene sheets is set to the same length and width.

Then, for the graphene closed-loop device system (Figure 2 (a)), the source and drain are shown in red box, and the dielectric and gate (located behind the dielectric) are shown in green box. The drain and source lengths were fixed at 4.92 \AA . The measurements of metal gate was fixed to $10.5 \text{ \AA} \times 8.5 \text{ \AA}$. Figures 1 (b) and (c) show the side view of the graphene device system. The value of dielectric $4\epsilon_0$ was chosen. Both types of bilayer graphene were stacked with a separation distance of 0.335 nm .

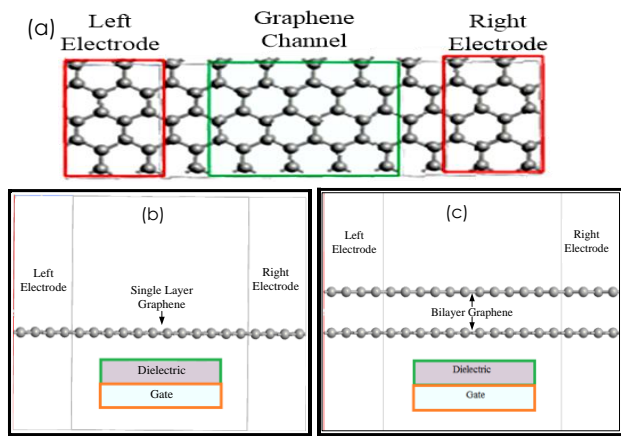


Figure 2: (a) The top view structure of the single and bilayer graphene closed loop system where the green box represents the dielectric and the red box at the right and left electrodes indicates the source and drain. (b) and (c) show the side view of the system. Clearly shows the dielectric and the gate of the system.

3. RESULTS AND DISCUSSION

3.1 Electronics properties of the graphene sheet

3.1.1 Band Structure

First, at zero bias voltage, assessments of the band structures and the DOS of the SLP, AA, and AB are computed. At point (the Brillouin zone's centre), structures for the band were simulated. The graphene sheet's axes of x, y, and z are included in the simulation. The y and z represent the graphene sheet's width and length, respectively, while the x and y stand for the sheet's layer.

Figure 2 displays the band configuration of the graphene sheets which the bandgap is calculated at point X. The band structure of the graphene sheets apparently changed. The energy level for conduction and valence band shifted (up and down from the 0 eV) respectively towards types of graphene (either single or bilayer). As for the SLP, both bands meet at 0 eV bandgap (Figure 2 (a)).

For the bilayer graphene sheet, the AA bandgap value is 1.701eV with an upper band value is 0.861 eV and a lower band value is -0.839 eV (Figure 2 (b)). Whilst for the AB, the bandgap is 1.854 eV (where the conduction band value is 0.956 eV, and the valence band value is -0.898eV (Figure 2 (c)). It is proven that the graphene band gap might be altered by the deformity of the structure or by adding the number of layers of the graphene [3]. Furthermore, the interlayer coupling effect the band structure depending on the number of

layers and stacking manner. The AB is energetically preferred over the AA in this scenario because of the bigger and more stable bandgap opening (owing to the Bernal stacked factor). The bandgap energy difference is 0.153 eV (about a 4.30% slight difference).

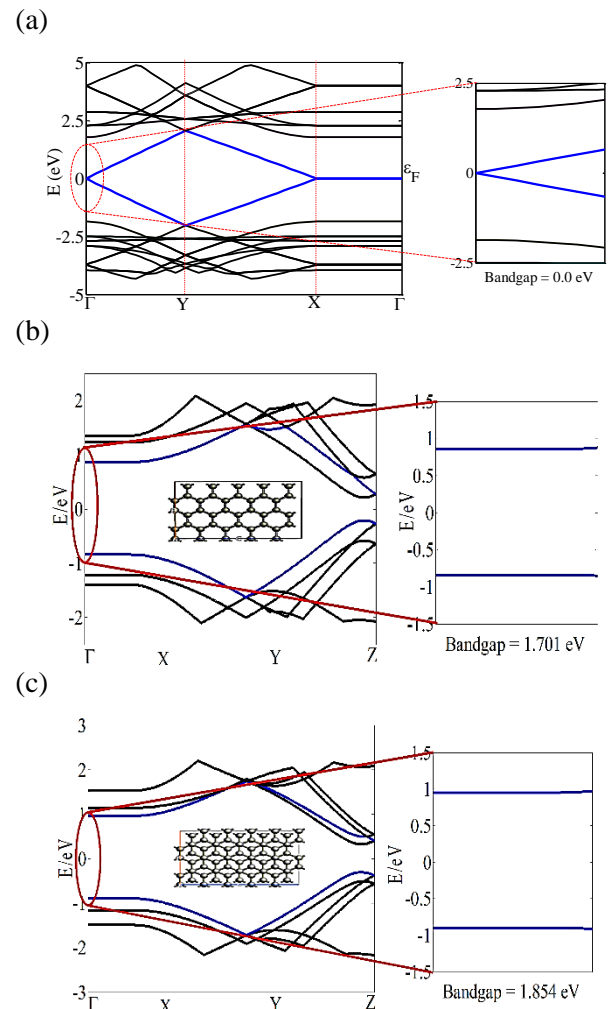


Figure 3: The band structures of (a) the SL pristine, (b) the AA-stacked pristine, and (c) the AB-stacked pristine. The inset of each diagram is the sheet image for SL pristine, AA-stacked pristine, and AB-stacked pristine respectively. Note that the bold blue color lines indicate the upper band (conduction band) and the lower band (valence band).

3.1.2 The Density of State (DOS)

Another property that garners a lot of interest is DOS. The DOS describes the number of states at a particular energy that an electron is free to occupy. Note that the DOS of graphene sheet is unlikely to other types of graphene structures (GNR, GNT, and many more). Each graphene sheet's DOS is plotted and shown in Figure 4. The trend of the waveform for SLP, AA, and AB are

nearly identical just with the existence of peaks for both bilayer graphene sheets. The DOS due to layers has a strong departure from the pristine (SLP) value close to the Dirac point. It is shown clearly by the existence of the peaks near the Dirac point for all graphene types except for SLP. It is believed that the abundance of peaks means more leaping electrons from the covalence band to the conductance band. The diminishing DOS at the Dirac point because there is no energy disparity between the bands of valence and conduction described the SLG as zero-band gap material [21].

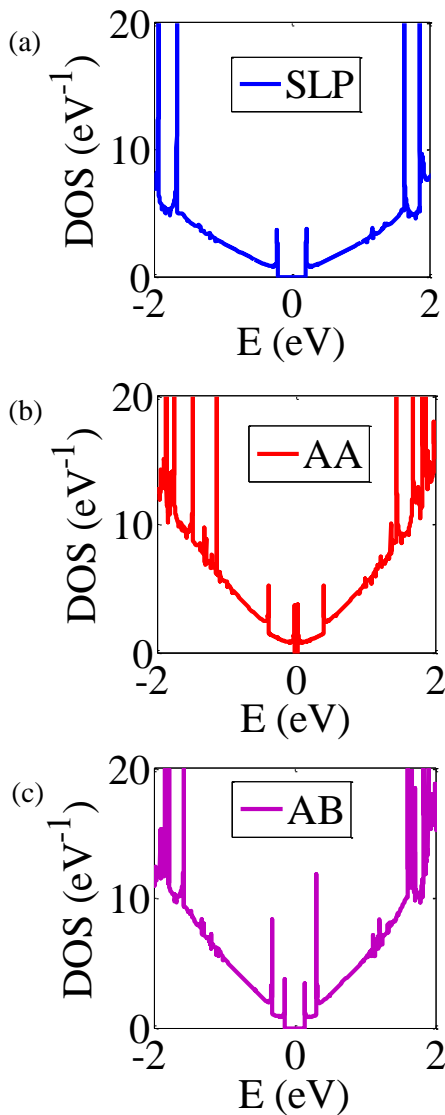


Figure 4: The density of state (DOS) per unit cell as a function of energy in units of eV of SLP, AA, and AB.

3.1.3 Transmission spectrum, conductance, and thermal conductance

The analyses are then continued with the transmission spectrum coefficient, the conductance coefficient, and thermal conductance coefficient. The transmission coefficient at energy E is obtained by summing up the transmission from all states.

$$T(E) = \sum_k t^\dagger t_k \delta(E - E_k)$$

Where t_k is the transmission amplitudes of a scattering state k which propagates through a device.

Figure 5 shows the value of the transmission spectrum coefficient for each type of graphene (single and bilayer). The transmission coefficient for AA and AB stacking graphene is above 4, showing the value of the transmission spectrum is doubled the SLP by the power of two.

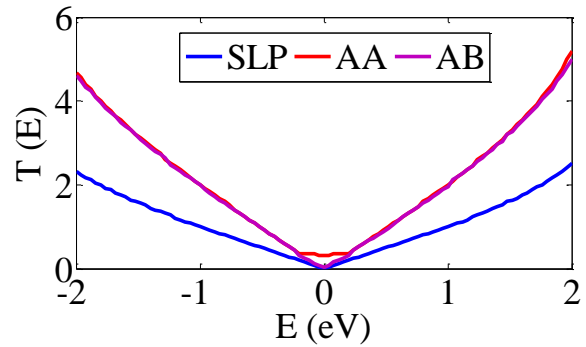


Figure 5: The transmission spectrum coefficient for graphene bulks. The overall spectrum shows that the pristine graphene (whether single or bilayer) shows a constant transmission coefficient.

Thermal conductance and conductance are the final stages of the simulation for transport characteristics (Figure 6(a) and (b)). As can be seen, the waveform trends for conductance and thermal conductance for each graphene sheet (single or bilayer) are quite comparable. (For instance, the definition of thermal conductance is the quantity of heat passing through a plate of a certain area and thickness in a unit of time when the temperatures on its opposing faces differ by one Kelvin). Figure 6(a) demonstrates how the conductance coefficient is reflected in the DOS values at the Fermi level.

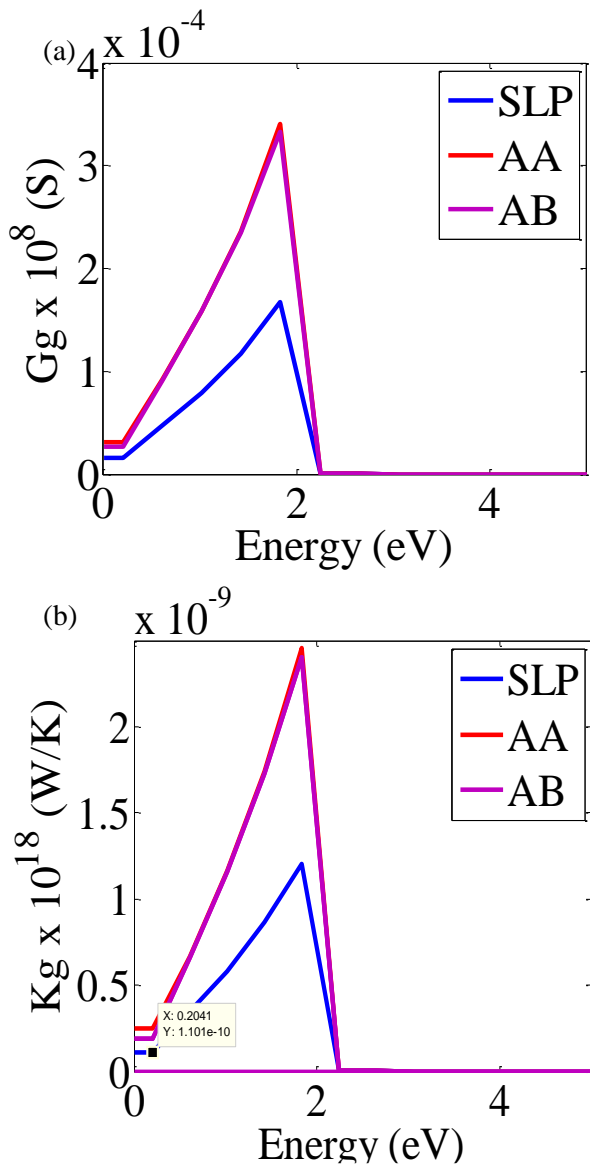


Figure 6: (a) The conductance coefficient and (b) the thermal conductance coefficient of the graphene bulk.

Lastly, as shown in Figure 6 (b), the thermal conductance for the AA is much greater compared to other graphene sheet types. The value of thermal conductance for both bilayer graphene shows doubled in value to the SLP.

3.2 Voltage-current characteristics

The performance of graphene in a back-gate design will be covered in this section. The bias voltage is set to 4 V to compare the efficacy of graphene devices. Ideal contact is thought to exist between the right electrode and the left electrode. The entire analysis is performed at the 300 K temperature setting at the 0 Fermi level.

For current-to-voltage curve devices performance, it can be seen how the graphene device saturated over time.

The much more interesting phenomenon is how the bilayer manipulates the device's performance. Figure 7 shows the current-voltage characteristic where the AB graphene device behaves like a conventional transistor with the off-state value before it starts to operate at $V \approx 0.3$ V. This situation is reflected in the conductance coefficient in Figure 6(a), where we can see the AB graphene sheet started at somewhere value like an SLP before it ramped up to the same value as AA graphene sheet. While for SLP and AA, the current-voltage characteristics start at 0V. The pattern of saturation looks the same for the bilayer graphene device and after some time, we can see the currents start to decline.

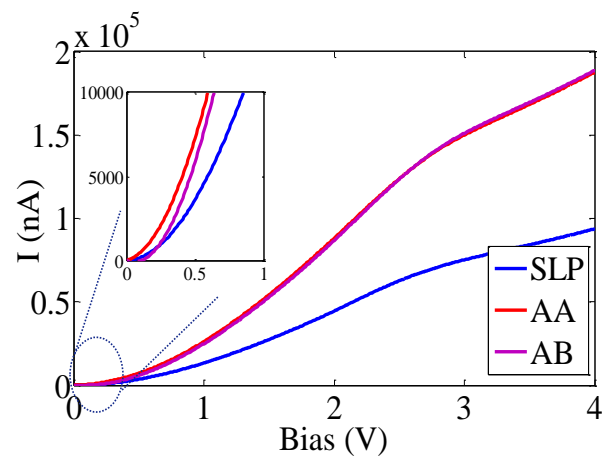


Figure 7: The current-voltage curve characteristics for pristine graphene devices (SLP, AA, and AB). The insert shows the ON condition for each graphene device.

4. CONCLUSIONS

This paper discusses an ab-initio study on single-layer graphene and bilayer graphene in both bulk and device forms. The study utilized two methods: the Extended-Huckel method and the Non-Equilibrium Green's Functional (NEGF) method. The findings of the study reveal interesting insights into the manipulation of the band structure and density of states in graphene sheets by employing bilayer graphene. Additionally, the transmission spectrum, which characterizes the behavior of carriers in graphene, is analyzed. The transmission spectrum also influences the reflection observed in the I-V (current-voltage) curves of the graphene device. Surprisingly, despite the introduction of an extra layer, the bilayer pristine graphene device demonstrates superior performance compared to the single-layer graphene device. This suggests that bilayer graphene has advantageous properties that make it a more favorable choice for certain applications.

Acknowledgment

The authors are truly grateful for the resources, facilities, and guidance provided by Politeknik Mersing and the School of Electrical Engineering, UTM. Their support has created an enabling environment for research excellence and has significantly enriched the quality of this project.

REFERENCES

- [1] K. S. Novoselov *et al.*, “Electric field effect in atomically thin carbon films.,” *Science*, vol. 306, no. 5696, pp. 666–669, Oct. 2004.
- [2] K. Matsumoto, K. Maehashi, Y. Ohno, and K. Inoue, “Recent advances in functional graphene biosensors,” *J. Phys. D. Appl. Phys.*, vol. 47, no. 9, p. 094005, Mar. 2014.
- [3] A. A. Balandin *et al.*, “Superior Thermal Conductivity of Single-Layer Graphene 2008,” *Nano Lett.*, vol. Vol.8, No., pp. 902–907, 2008.
- [4] M. Pumera, “Graphene in biosensing,” *Mater. Today*, vol. 14, no. 7–8, pp. 308–315, Jul. 2011.
- [5] L. Liang *et al.*, “Theoretical studies on the dynamics of DNA fragment translocation through multilayer graphene nanopores,” *RSC Adv.*, vol. 4, no. 92, pp. 50494–50502, Oct. 2014.
- [6] M. Junaid and G. Witjaksono, “Analysis of band gap in AA and Ab stacked bilayer graphene by Hamiltonian tight binding method,” *2019 IEEE Int. Conf. Sensors Nanotechnology, SENSORS NANO 2019*, no. July, 2019.
- [7] X. Liang, Z. A. H. Goodwin, V. Vitale, F. Corsetti, A. A. Mostofi, and J. Lischner, “Effect of bilayer stacking on the atomic and electronic structure of twisted double bilayer graphene,” *Phys. Rev. B*, vol. 102, no. 15, pp. 1–14, 2020.
- [8] M. Yankowitz *et al.*, “Tuning superconductivity in twisted bilayer graphene,” *Science (80-.)*, vol. 363, no. 6431, pp. 1059–1064, 2019.
- [9] J. Ruseckas, A. Mekys, G. Juzeliūnas, and I. V. Zouzoulenko, “Electron transmission through graphene monolayer-bilayer junction: An analytical approach,” *Lith. J. Phys.*, vol. 52, no. 1, pp. 70–80, 2012.
- [10] A. J. Schmidt, K. C. Collins, A. J. Minnich, and G. Chen, “Thermal conductance and phonon transmissivity of metal–graphite interfaces,” *J. Appl. Phys.*, vol. 107, no. 10, p. 104907, 2010.
- [11] H. Yang, Y. Tang, Y. Liu, X. Yu, and P. Yang, “Thermal conductivity of graphene nanoribbons with defects and nitrogen doping,” *React. Funct. Polym.*, vol. 79, pp. 29–35, Jun. 2014.
- [12] J. Yang *et al.*, “Thermal conductance imaging of graphene contacts,” *J. Appl. Phys.*, vol. 116, no. 2, p. 023515, Jul. 2014.
- [13] S. D. Costa, J. Ek Weis, O. Frank, and M. Kalbac, “Effect of layer number and layer stacking registry on the formation and quantification of defects in graphene,” *Carbon N. Y.*, vol. 98, pp. 592–598, Mar. 2016.
- [14] P. Willke *et al.*, “Doping of Graphene by Low-Energy Ion Beam Implantation: Structural, Electronic, and Transport Properties,” *Nano Lett.*, vol. 15, no. 8, 2015.
- [15] I. Bertóti, M. Mohai, and K. László, “Surface modification of graphene and graphite by nitrogen plasma: Determination of chemical state alterations and assignments by quantitative X-ray photoelectron spectroscopy,” *Carbon N. Y.*, vol. 84, no. 1, pp. 185–196, 2015.
- [16] S. Awasthi, P. S. Gopinathan, A. Rajanikanth, and C. Bansal, “SC,” *J. Sci. Adv. Mater. Devices*, 2018.
- [17] L. Han *et al.*, “In-Plane Carbon Lattice-Defect Regulating Electrochemical Oxygen Reduction to Hydrogen Peroxide Production over Nitrogen-Doped Graphene,” *ACS Catal.*, vol. 9, no. 2, pp. 1283–1288, 2019.
- [18] M. Morsin and Y. Yusof, “The Ab-initio study of bulk single layer defected graphene towards graphene device,” *Int. J. Electr. Comput. Eng.*, vol. 7, no. 3, pp. 1444–1451, 2017.
- [19] *Atomistix ToolKit Manual (Version 13.8)*. .
- [20] J.-W. Jiang, J.-S. Wang, and B.-S. Wang, “Minimum thermal conductance in graphene and boron nitride superlattice,” *Appl. Phys. Lett.*, vol. 99, no. 4, p. 043109, 2011.
- [21] C. S. Allen and J. H. Warner, *Graphene*, no. 2009. 2013.